Physics Letters B 699 (2011) 330–340

Contents lists available at ScienceDirect

Physics Letters B

www.elsevier.com/locate/physletb

Search for the rare decays $B_s^0 \to \mu^+\mu^-$ and $B^0 \to \mu^+\mu^-$ ☆

LHCb Collaboration

ARTICLE INFO

Article history:
Received 13 March 2011
Received in revised form 12 April 2011
Accepted 13 April 2011
Available online 20 April 2011
Editor: W.-D. Schlatter

Keywords:
LHC
b-Hadron
FCNC
Rare decays
Leptonic decays

ABSTRACT

A search for the decays $B_s^0 \to \mu^+\mu^-$ and $B^0 \to \mu^+\mu^-$ is performed with about 37 pb^{-1} of pp collisions at $\sqrt{s} = 7$ TeV collected by the LHCb experiment at the Large Hadron Collider at CERN. The observed numbers of events are consistent with the background expectations. The resulting upper limits on the branching ratios are $\mathcal{B}(B_s^0 \to \mu^+\mu^-) < 5.6 \times 10^{-8}$ and $\mathcal{B}(B^0 \to \mu^+\mu^-) < 1.5 \times 10^{-8}$ at 95% confidence level.

1. Introduction

Within the Standard Model (SM) exclusive dimuon decays of the B^0 and B_s^0 mesons[1] are rare as they occur only via loop diagrams and are helicity suppressed. New Physics models, especially those with an extended Higgs sector, can significantly enhance the branching fractions, although in some models the rates are lowered.

The amplitudes contributing to the branching ratio $\mathcal{B}(B_q^0 \to \mu^+\mu^-)$ (where $q = d, s$ for the B^0 and B_s^0 mesons respectively) can be expressed in terms of the scalar (c_S), pseudoscalar (c_P) and axial vector (c_A) Wilson coefficients in a completely general approach [1]. Within the SM, the contributions of c_S and c_P are negligible while c_A is calculated with an accuracy of a few percent [2]. The dominant contribution stems from an electroweak penguin with a Z^0 decaying into two muons. However, the accuracy of the SM prediction for $\mathcal{B}(B_q^0 \to \mu^+\mu^-)$ is limited by the knowledge of the decay constants of the B_q^0 mesons. This limitation can be reduced by normalizing to the well-measured mass differences of the B_q^0 mesons. Using this approach [3], the SM predictions are

$$\mathcal{B}\left(B_s^0 \to \mu^+\mu^-\right)_{\mathrm{SM}} = (0.32 \pm 0.02) \times 10^{-8},$$
$$\mathcal{B}\left(B^0 \to \mu^+\mu^-\right)_{\mathrm{SM}} = (0.010 \pm 0.001) \times 10^{-8}.$$

Many extensions to the SM predict a very different Higgs sector. For instance, within the Minimal Supersymmetric SM (MSSM) in the large $\tan\beta$ approximation [4], $c_{S,P}^{\mathrm{MSSM}} \propto \tan^3\beta / M_A^2$, where M_A denotes the pseudoscalar Higgs mass and $\tan\beta$ the ratio of Higgs vacuum expectation values. The most restrictive limits on the search for $B_q^0 \to \mu^+\mu^-$ have so far been achieved at the Tevatron, due to the large $b\bar{b}$ cross-section at hadron colliders. The best limits at 95% C.L. published so far are obtained using 6.1 fb^{-1} by the D0 Collaboration [5], $\mathcal{B}(B_s^0 \to \mu^+\mu^-) < 5.1 \times 10^{-8}$, and using 2 fb^{-1} by the CDF Collaboration [6], $\mathcal{B}(B_s^0 \to \mu^+\mu^-) < 5.8 \times 10^{-8}$ and $\mathcal{B}(B^0 \to \mu^+\mu^-) < 1.8 \times 10^{-8}$. The CDF Collaboration has also presented preliminary results [7] with 3.7 fb^{-1}, that lower the limits to $\mathcal{B}(B_s^0 \to \mu^+\mu^-) < 4.3 \times 10^{-8}$ and $\mathcal{B}(B^0 \to \mu^+\mu^-) < 0.76 \times 10^{-8}$.

The LHCb experiment is well suited for such searches due to its good invariant mass resolution, vertex resolution, muon identification and trigger acceptance. In addition, LHCb has a hadronic trigger capability which provides large samples of $B_q^0 \to h^+h'^-$ decays, where h and h' stand for a hadron (kaon or pion). These are used as control samples in order to reduce the dependence of the results on the simulation.

The measurements in this Letter use about 37 pb^{-1} of integrated luminosity collected by LHCb between July and October 2010 at $\sqrt{s} = 7$ TeV. Assuming the SM branching ratio, about 0.7 (0.08) $B_s^0 \to \mu^+\mu^-$ ($B^0 \to \mu^+\mu^-$) are expected to be reconstructed using the $b\bar{b}$ cross-section, measured within the LHCb acceptance, of 75 ± 14 μb [8].

2. The LHCb detector

The LHCb detector [9] is a single-arm forward spectrometer with an angular coverage from approximately 10 mrad to 300

☆ © CERN, for the benefit of the LHCb Collaboration.

[1] In this Letter the inclusion of charge-conjugate states is implicit.

0370-2693
doi:10.1016/j.physletb.2011.04.031

(250) mrad in the bending (non-bending) plane. The detector consists of a vertex locator (VELO), a warm dipole magnet with a bending power of $\int B\,dl = 4$ Tm, a tracking system, two ring-imaging Cherenkov detectors (RICH), a calorimeter system and a muon system. The VELO consists of a series of silicon modules, each providing a measure of the radial and azimuthal coordinates, with the sensitive area starting at 8 mm from the beam line during collisions. The tracking system comprises four layers of silicon sensors before the magnet and three stations equipped with silicon sensors in the inner part and straw tubes in the outer part after the magnet. Track momenta are measured with a precision between $\delta p/p = 0.35\%$ at 5 GeV/c and $\delta p/p = 0.5\%$ at 100 GeV/c. The RICH system provides charged hadron identification in a momentum range 2–100 GeV/c. The calorimeter system consists of a preshower, a scintillating pad detector, an electromagnetic calorimeter and a hadronic calorimeter. It identifies high transverse energy ($E_{\rm T}$) hadron, electron and photon candidates and provides information for the trigger. Five muon stations composed of MWPC (except in the highest rate region, where triple-GEMs are used) provide fast information for the trigger and muon identification capability.

LHCb has a two-level trigger system both for leptonic and purely hadronic final states. It exploits the finite lifetime and relatively large mass of charm and beauty hadrons to distinguish heavy flavour decays from the dominant light quark processes. The first trigger level (L0) is implemented in hardware and reduces the rate to a maximum of 1 MHz, the read-out rate of the whole detector. The second trigger level (High Level Trigger, HLT) is implemented in software running on an event filter CPU farm. In the first stage of the software trigger (HLT1) a partial event reconstruction is performed. The second stage (HLT2) performs a full event reconstruction to enhance the signal purity further.

The forward geometry of LHCb allows the first level trigger to collect events containing one or two muons with very low transverse momenta ($p_{\rm T}$): more than 90% of the data were collected with a $p_{\rm T}$ threshold of 1.4 GeV/c for single muon triggers and $p_{\rm T}(\mu_1) > 0.48$ GeV/c and $p_{\rm T}(\mu_2) > 0.56$ GeV/c for dimuon triggers. The $E_{\rm T}$ threshold for the hadron trigger varied in the range 2.6 to 3.6 GeV. The single muon trigger line in the HLT requires either $p_{\rm T} > 1.8$ GeV/c or includes a cut on the impact parameter (IP) with respect to the primary vertex, which allows for a lower $p_{\rm T}$ requirement ($p_{\rm T} > 0.8$ GeV/c, IP > 0.11 mm). The dimuon trigger line requires muon pairs of opposite charge forming a common vertex and an invariant mass $M_{\mu\mu} > 4.7$ GeV/c^2. A second trigger line, primarily to select J/ψ events, requires $2.97 < M_{\mu\mu} < 3.21$ GeV/c^2. The remaining region of the dimuon invariant mass is also covered by trigger lines that in addition require the dimuon secondary vertex to be well separated from the primary vertex. Other HLT trigger lines select generic displaced vertices, providing a high efficiency for purely hadronic decays (for instance $B_q^0 \to h^+h'^-$).

3. Analysis strategy

An important feature of this analysis is to rely as much as possible on data and to restrict to a minimum the use of simulation. Nevertheless, some Monte Carlo (MC) simulation has been used, based on the PYTHIA 6.4 generator [11] and the GEANT4 package [12] for detector simulation. The first part of the analysis is the event selection (Section 4), which significantly reduces the size of the dataset by rejecting most of the background.

The second part consists of the study of three normalization channels with known branching ratios: $B^+ \to J/\psi(\mu^+\mu^-)K^+$, $B_s^0 \to J/\psi(\mu^+\mu^-)\phi(K^+K^-)$ and $B^0 \to K^+\pi^-$. Using each of these normalization channels, $\mathcal{B}(B_q^0 \to \mu^+\mu^-)$ can be calculated as:

$$\begin{aligned}\mathcal{B}\big(B_q^0 \to \mu^+\mu^-\big) &= \mathcal{B}_{\rm norm} \times \frac{\epsilon_{\rm norm}^{\rm REC}\epsilon_{\rm norm}^{\rm SEL|REC}\epsilon_{\rm norm}^{\rm TRIG|SEL}}{\epsilon_{\rm sig}^{\rm REC}\epsilon_{\rm sig}^{\rm SEL|REC}\epsilon_{\rm sig}^{\rm TRIG|SEL}} \times \frac{f_{\rm norm}}{f_{B_q^0}} \times \frac{N_{B_q^0\to\mu^+\mu^-}}{N_{\rm norm}} \\ &= \alpha_{B_q^0\to\mu^+\mu^-} \times N_{B_q^0\to\mu^+\mu^-}, \end{aligned} \quad (1)$$

where $\alpha_{B_q^0\to\mu^+\mu^-}$ denotes the normalization factor, $f_{B_q^0}$ denotes the probability that a b-quark fragments into a B_q^0 and $f_{\rm norm}$ denotes the probability that a b-quark fragments into the b-hadron relevant for the chosen normalization channel with branching fraction $\mathcal{B}_{\rm norm}$. The reconstruction efficiency ($\epsilon^{\rm REC}$) includes the acceptance and particle identification, while $\epsilon^{\rm SEL|REC}$ denotes the selection efficiency on reconstructed events. The trigger efficiency on selected events is denoted by $\epsilon^{\rm TRIG|SEL}$. This normalization ensures that knowledge of the absolute luminosity and $b\bar{b}$ production cross-section are not needed, and that many systematic uncertainties cancel in the ratio of the efficiencies. The event selection for these channels is specifically designed to be as close as possible to the signal selection. The ratios of reconstruction and selection efficiencies are estimated from the simulation, while the ratios of trigger efficiencies on selected events are determined from data (Section 5).

In the third part of the analysis (Section 6) each selected event is given a probability to be signal or background in a two-dimensional probability space defined by the dimuon invariant mass and a geometrical likelihood (GL). The dimuon invariant mass and GL probability density functions for both signal and background are determined from data. This procedure ensures that even though the GL is defined using simulated events, the result will not be biased by discrepancies between data and simulation.

Section 7 describes the final measurement. In order to avoid unconscious bias in the analysis, the invariant mass region for the signal ($M_{B^0} \pm 60$ MeV/c^2 and $M_{B_s^0} \pm 60$ MeV/c^2) was blinded until the selection criteria and analysis procedure had been defined.

4. Event selection

The selection has been designed in order to reduce the data sample to a manageable level by simultaneously keeping the efficiency for the signals as high as possible and the selection between signals and control channels as similar as possible. This last requirement is needed to minimize the systematic uncertainty in the ratio of the selection efficiencies. The optimal separation between signal and background is left to the likelihoods (Section 6). The basic cuts of the selection have been defined on Monte Carlo simulation [10] and then adapted to the data.

The data for the signal and all the normalization candidates are selected using either an inclusive two-body or a J/ψ selection. Tracks are first required to be of good quality ($\chi^2/{\rm ndf} < 5$) and to be displaced with respect to the closest primary vertex ($\chi^2_{\rm IP}/{\rm ndf} > 12.5$, where $\chi^2_{\rm IP}$ is the difference between the χ^2 of the primary vertex built with and without the considered track). To reject bad combinations before performing the vertex fit, the two tracks are required to have a distance of closest approach of less than 0.3 mm. The secondary vertex is required to be well fitted ($\chi^2/{\rm ndf} < 9$) and must be clearly separated from the primary in the forward direction (vertex distance significance larger than 15). When more than one primary vertex is reconstructed, the one that gives the minimum impact parameter significance for the candidate is chosen. The reconstructed candidate has to point to the primary vertex ($\chi^2_{\rm IP}/{\rm ndf} < 12.5$) in the case of the inclusive two-body selection. For all selections, the primary vertex is refit-

Table 1
Summary of the factors and their uncertainties needed to calculate the normalization factors ($\alpha_{B_q^0\to\mu^+\mu^-}$) for the three normalization channels considered. The branching ratios are taken from Refs. [14,16]. The trigger efficiency and number of $B^0\to K^+\pi^-$ candidates correspond to only TIS events, as described in the text.

	$\mathcal{B}$ ($\times10^{-5}$)	$\frac{\epsilon^{\rm REC}_{\rm norm}\epsilon^{\rm SEL|REC}_{\rm norm}}{\epsilon^{\rm REC}_{\rm sig}\epsilon^{\rm SEL|REC}_{\rm sig}}$	$\frac{\epsilon^{\rm TRIG|SEL}_{\rm norm}}{\epsilon^{\rm TRIG|SEL}_{\rm sig}}$	$N_{\rm norm}$	$\alpha_{B_s^0\to\mu^+\mu^-}$ ($\times10^{-9}$)	$\alpha_{B^0\to\mu^+\mu^-}$ ($\times10^{-9}$)
$B^+\to J/\psi(\mu^+\mu^-)K^+$	5.98 ± 0.22	0.49 ± 0.02	0.96 ± 0.05	$12{,}366\pm403$	8.4 ± 1.3	2.27 ± 0.18
$B_s^0\to J/\psi(\mu^+\mu^-)\phi(K^+K^-)$	3.4 ± 0.9	0.25 ± 0.02	0.96 ± 0.05	760 ± 71	10.5 ± 2.9	2.83 ± 0.86
$B^0\to K^+\pi^-$	1.94 ± 0.06	0.82 ± 0.06	0.072 ± 0.010	578 ± 74	7.3 ± 1.8	1.99 ± 0.40

ted excluding the signal tracks before calculating the $\chi^2_{\rm IP}$/ndf and the vertex distance significance of the candidate.

Tracks are defined as muons if they have at least one hit in two to four of the last four muon stations depending on the momentum. In the inclusive J/ψ selection both tracks must be identified as muons and have an invariant mass within 60 MeV/c^2 of the nominal J/ψ mass. The efficiency of the muon identification requirement has been measured using an inclusive sample of J/ψ events where one of the tracks does not use any information from the muon chambers. The efficiency measured with data agrees with MC expectations as a function of momentum within 2%, and the residual differences are taken into account in the systematic uncertainties.

Events passing the two-body selection are considered $B_q^0\to\mu^+\mu^-$ candidates if both tracks pass the muon identification criteria, and their invariant mass lies within 60 MeV/c^2 of the nominal B_q^0 mass. The invariant mass of the $B_q^0\to h^+h'^-$ candidates has to be within 600 MeV/c^2 of the nominal B_q^0 mass. As the acceptance of the tracking stations is larger than the muon chambers, the selected $B_q^0\to h^+h'^-$ candidates are required to have both tracks within the muon chamber acceptance to minimize the differences with $B_q^0\to\mu^+\mu^-$. The total efficiencies including acceptance, reconstruction and selection criteria on MC $B_q^0\to\mu^+\mu^-$ and $B_q^0\to h^+h'^-$ events are 5.5% and 4.5% respectively; the main difference is due to material interactions. Assuming the SM branching ratio, 0.3 $B_s^0\to\mu^+\mu^-$ and 0.04 $B^0\to\mu^+\mu^-$ events are expected after all selection requirements. There are 343 (342) $B_q^0\to\mu^+\mu^-$ candidates selected from data in the B_s^0 (B^0) mass window.

The dominant background after the $B_q^0\to\mu^+\mu^-$ selection is expected to be $b\bar{b}\to\mu\mu X$ [10,13]. This is confirmed by comparing the kinematical distributions of the sideband data with a $b\bar{b}\to\mu\mu X$ MC sample. The muon misidentification probability as a function of momentum obtained from data using $K_S^0\to\pi^+\pi^-$, $\Lambda\to p\pi^-$ and $\phi\to K^+K^-$ decays is in good agreement with MC expectations. An estimate of the background coming from misidentified hadrons is obtained by reweighting the hadron misidentification probability using the momentum spectrum of the background in the invariant mass sidebands. The single hadron average misidentification probability is measured to be $(7.1\pm0.5)\times10^{-3}$ and the double hadron misidentification probability is $(3.5\pm0.9)\times10^{-5}$, where the correlation between the momenta of the two hadrons is taken into account. About 10% of the background is due to pairs consisting of one real muon and a hadron misidentified as muon, mostly from decays in flight. The contribution from double misidentified hadrons is negligible. The number of expected $B_q^0\to h^+h'^-$ candidates misidentified as $B_q^0\to\mu^+\mu^-$ within the search window of ±60 MeV/c^2 around the B_s^0 (B^0) mass is less than 0.1 (0.3).

For the $B^+\to J/\psi K^+$ and $B_s^0\to J/\psi\phi$ normalization channels some additional cuts are required. In the former case, the $K^\pm$ candidates are required to pass the same track quality and impact parameter cuts as the muons from the J/ψ. For $B_s^0\to J/\psi\phi$ candidates, the K^+K^- invariant mass is required to be within ±10 MeV/c^2 of the ϕ mass [14]. The B vertex has to be of good quality, χ^2/ndf <25. The requirements on $\chi^2_{\rm IP}$/ndf and vertex separation significance for the B candidate are the same as those for the signal selection. The total efficiencies including acceptance, reconstruction and selection criteria for MC $B^+\to J/\psi K^+$ and $B_s^0\to J/\psi\phi$ events are 2.6% and 1.3% respectively.

5. Evaluation of the normalization factor

The branching fractions of the three normalization channels, $B^+\to J/\psi(\mu^+\mu^-)K^+$, $B_s^0\to J/\psi(\mu^+\mu^-)\phi(K^+K^-)$ and $B^0\to K^+\pi^-$, are shown in Table 1. The first two decays have similar trigger and muon identification efficiency to the signal but a different number of particles in the final state, while the third channel has the same two-body topology but is selected with the hadronic trigger. The branching ratio of the $B_s^0\to J/\psi\phi$ decay is not known precisely ($\sim25\%$) but has the advantage that the normalization of $B_s^0\to\mu^+\mu^-$ with a B_s^0 decay does not require the knowledge of the ratio of fragmentation fractions, which has an uncertainty of $\sim13\%$ [15].

5.1. Ratio of reconstruction and selection efficiencies

The accuracy of the simulation of the reconstruction efficiency $\epsilon^{\rm REC}$ relies on the knowledge of the detector geometrical acceptance, the material interactions and the tracking efficiency. The uncertainty on the tracking efficiency is taken to be 4% per track [8] and this is the dominant source of the systematic uncertainty in the ratio with the two normalization channels involving J/ψ mesons. The ratios $\epsilon^{\rm REC}_{\rm norm}/\epsilon^{\rm REC}_{\rm sig}$ predicted by the simulation are 0.58 ± 0.02 ($B^+\to J/\psi K^+$), 0.39 ± 0.03 ($B_s^0\to J/\psi\phi$) and 0.75 ± 0.05 ($B^0\to K^+\pi^-$).

The effect of an extra particle on the ratio of $\epsilon^{\rm REC}$ is cross-checked in data using the decay $B^0\to J/\psi(\mu^+\mu^-)K^{*0}(K^+\pi^-)$. Selecting B^0 and B^+ in a similar phase-space region, the ratio of $B^0\to J/\psi K^{*0}$ and $B^+\to J/\psi K^+$ yields (corrected for the ratio of branching ratios) is a good measure of the ratio of $\epsilon^{\rm REC}$ between $B^+\to J/\psi K^+$ and $B_q^0\to\mu^+\mu^-$, as shown in Ref. [10]. The measurement from data is 0.59 ± 0.04, in good agreement with the estimate from MC simulation (0.58 ± 0.02).

The accuracy of the simulation of $\epsilon^{\rm SEL|REC}$ relies on how well the MC describes the variables entering the selection. Of these only the IP distributions show a significant discrepancy: the data are measured to have $\sim10\%$ worse resolution than the simulation. Smearing the track parameters in MC to reproduce the IP distribution in data changes the selection efficiencies by 5–7% depending on the channel. However, the ratios of $\epsilon^{\rm SEL|REC}_{\rm norm}/\epsilon^{\rm SEL|REC}_{\rm sig}$ remain unchanged within the MC statistical uncertainty. The ratios predicted by the MC are 0.85 ± 0.01 ($B^+\to J/\psi K^+$), 0.63 ± 0.01 ($B_s^0\to J/\psi\phi$) and 1.09 ± 0.01 ($B^0\to K^+\pi^-$), where the uncertainties correspond to the MC statistical uncertainties. The largest contribution to the difference in the selection efficiencies for $B^+\to J/\psi K^+$ and $B_s^0\to J/\psi\phi$ compared to the signal comes from the additional $\chi^2_{\rm IP}$ requirements on the extra tracks in the normalization channels. For the $B^0\to K^+\pi^-$ normalization channel, the selection

efficiency is higher than for the signal as the tight (± 60 MeV/c^2) mass window is not applied to the $B_q^0 \to h^+h'^-$ channel. The ratios of efficiencies including acceptance, reconstruction and selection between normalization and signal decays are shown in Table 1.

5.2. Ratio of trigger efficiencies

The trigger efficiency $\epsilon^{\text{TRIG|SEL}}$ can be estimated from data as described in Ref. [10]. Events that would have triggered even without the presence of the decay products of the signal under study are tagged as TIS events (Trigger Independent of Signal). TIS events are mostly triggered by the decay products of the other b which can be in the acceptance given the forward geometry of LHCb.

If the presence of the signal under study alone is sufficient to trigger, events are tagged as TOS (Trigger On Signal). An event can also be TIS and TOS simultaneously (TIS&TOS). The overall trigger efficiency on selected events can then be expressed as:

$$\epsilon^{\text{TRIG|SEL}} = \frac{N^{\text{TRIG}}}{N^{\text{SEL}}} = \frac{N^{\text{TIS}}}{N^{\text{SEL}}}\frac{N^{\text{TRIG}}}{N^{\text{TIS}}} = \epsilon^{\text{TIS}}\frac{N^{\text{TRIG}}}{N^{\text{TIS}}}, \tag{2}$$

where N^{SEL} is not directly observable as it corresponds to a sample of selected events for a fully efficient trigger. The TIS efficiency (ϵ^{TIS}) can however be measured directly on data using the ratio $N^{\text{TIS\&TOS}}/N^{\text{TOS}}$. Therefore $\epsilon^{\text{TRIG|SEL}}$ can be expressed in terms of fully observable quantities.

The trigger efficiency for selecting $B^+ \to J/\psi K^+$ and $B_s^0 \to J/\psi\phi$ is obtained from a large inclusive sample of J/ψ events using Eq. (2). The result is $\epsilon_{J/\psi}^{\text{TRIG|SEL}} = (85.9 \pm 0.9_{\text{stat}} \pm 2.0_{\text{syst}})\%$, where the systematic uncertainty reflects the approximation of the method as seen in the simulation. This efficiency is parameterized as a function of the largest p_{T} and the largest IP of the two muons. Using the phase space of the $B_q^0 \to \mu^+\mu^-$ decay in these two variables, the trigger efficiency for the signal is evaluated to be $\epsilon_{B_q^0\to\mu^+\mu^-}^{\text{TRIG|SEL}} = (89.9 \pm 0.8_{\text{stat}} \pm 4.0_{\text{syst}})\%$, where the systematic uncertainty is increased to account for the limitations of using only two variables (the largest p_{T} and IP of the muons in the final state) to parameterize the trigger response.

In the case of the $B^0 \to K^+\pi^-$ normalization channel, the trigger efficiency is computed using the same events that are used for the normalization in Eq. (1). Therefore, combining Eqs. (1) and (2) results in an expression equivalent to a normalization which uses only TIS events. The total number of these events after the first trigger steps (L0 and HLT1) is 578, accepting all HLT2 triggers, which does not allow for a precise measurement of ϵ^{TIS}. Instead, this efficiency can be measured using another control channel, $B^+ \to J/\psi K^+$, with the result: $\epsilon^{\text{TIS}}(\text{L0} \times \text{HLT1}) = (6.9 \pm 0.6)\%$. The small correction due to the HLT2 trigger inefficiency on selected $B^0 \to K^+\pi^-$ candidates is taken from the trigger emulation. The ratios $\epsilon_{\text{norm}}^{\text{TRIG|SEL}}/\epsilon_{\text{sig}}^{\text{TRIG|SEL}}$ for the three normalization channels are given in Table 1.

5.3. Overall normalization factor

The yields needed to evaluate the normalization factor for the two channels containing a J/ψ in the final state are obtained from a Gaussian fit to the invariant mass distribution. The number of candidates can be seen in Table 1, where the uncertainty is dominated by the differences observed using different fitting models. In the case of the $B^0 \to K^+\pi^-$ decay, the RICH particle identification and mass information are used to extract the fraction of $K^+\pi^-$ events from the selected inclusive $B_q^0 \to h^+h'^-$ sample. The efficiency of the kaon and pion identification requirements is not needed since their ratio is extracted from the known ratio of $B^0 \to \pi^+\pi^-$ and $B^0 \to K^+\pi^-$ branching ratios as described in Ref. [10]. The number of TIS $B^0 \to K^+\pi^-$ events observed is shown in Table 1.

As can be seen in Table 1, the normalization factors calculated using the three complementary channels give compatible results. The final normalization factor is a weighted average which takes into account all the sources of correlations, in particular the dominant one coming from the uncertainty on $f_d/f_s = 3.71 \pm 0.47$ [15], with the result:

$$\alpha_{B_s^0\to\mu^+\mu^-} = (8.6 \pm 1.1) \times 10^{-9},$$
$$\alpha_{B^0\to\mu^+\mu^-} = (2.24 \pm 0.16) \times 10^{-9}.$$

6. Signal and background likelihoods

After the selection described in Section 4 the signal purity assuming the SM branching ratio is still about 10^{-3} for $B_s^0 \to \mu^+\mu^-$ and 10^{-4} for $B^0 \to \mu^+\mu^-$. Further discrimination is achieved through the combination of two independent variables: the multivariate analysis discriminant likelihood, GL, combining information that is largely based on the topology of the event, and the invariant mass. The GL is defined using the statistical method described in Refs. [13,17]. The GL is defined to have a flat distribution between zero and one for signal candidates, and to cluster around zero for background candidates. The geometrical variables included in the definition of the GL are intended to be a complete set describing the properties of the decay, and the transverse momentum of the B candidate is also included, which is uncorrelated with the invariant mass. The variables used in the definition of the GL are:

- *Lifetime of the B candidate*. This variable is computed using the distance between the secondary vertex and primary vertex, and the reconstructed momentum of the B candidate. When more than one primary vertex is reconstructed, the one that gives the minimum B impact parameter significance is chosen.
- *Muon impact parameter* χ^2. This is the lowest impact parameter χ^2 of the two muon candidates with respect to any primary vertex reconstructed in the event.
- *Impact parameter of the B candidate*.
- *Distance of closest approach between the two muon candidates*.
- *Isolation*. For each of the muon candidates, a search is performed for other tracks that can make a good vertex with the muon candidate, as in Ref. [10]. The number of compatible tracks is used as the discriminant variable.
- *Transverse momentum of the B candidate*.

The analysis is performed in two-dimensional bins of invariant mass and GL. The invariant mass in the signal regions (± 60 MeV/c^2 around the B_s^0 and the B^0 masses) is divided into six bins of equal width, and the GL into four bins of equal width distributed between zero and one. A probability to be signal or background is assigned to events falling in each bin.

6.1. Signal geometrical likelihood

Although the GL variable described above was defined using MC events, the probability that a signal event has a given value of GL is obtained from data using inclusive $B_q^0 \to h^+h'^-$ events. Studies with large samples of MC events show that after reconstruction and selection the GL distributions obtained from $B_q^0 \to \mu^+\mu^-$ and $B_q^0 \to h^+h'^-$ signal events agree within uncertainties (3%). On the other hand, the two distributions are different after the trigger is emulated. This bias can be removed if only TIS $B_q^0 \to h^+h'^-$ events are used in the evaluation of the GL distribution. However, the total number of TIS $B_q^0 \to h^+h'^-$ events after all trigger steps (L0, HLT1

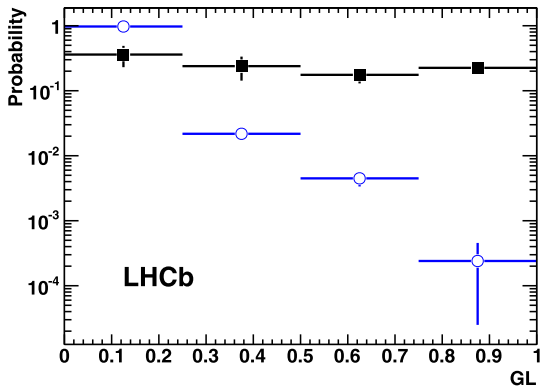

Fig. 1. Probability of signal events in bins of GL obtained from the inclusive sample of TIS $B_q^0 \to h^+h'^-$ events (solid squares). The background probability (open circles) is obtained from the events in the sidebands of the $\mu\mu$ invariant mass distribution in the B_s^0 mass window.

Table 2
Probability of signal events in bins of GL obtained from the inclusive sample of TIS $B_q^0 \to h^+h'^-$ events. The background probability in the B_s^0 mass window is obtained from the events in the sidebands of the dimuon invariant mass distribution.

GL bin	Signal prob.	Background prob.
0.0–0.25	0.360 ± 0.130	$0.9735^{+0.0030}_{-0.0032}$
0.25–0.5	0.239 ± 0.096	$0.0218^{+0.0030}_{-0.0028}$
0.5–0.75	0.176 ± 0.046	$0.0045^{+0.0012}_{-0.0010}$
0.75–1.0	0.225 ± 0.036	$0.00024^{+0.00031}_{-0.00015}$

and HLT2) is 152 which is insufficient. Instead, for the $B_q^0 \to h^+h'^-$ events, the first two trigger steps (L0 and HLT1) are required to be TIS while at the HLT2 step any of the HLT2 triggers are accepted. This yields 955 events. The GL distribution obtained using these events is corrected for the small bias ($< 5\%$) introduced at the HLT2 stage using the trigger emulation. Detailed checks with a large sample of $D^0 \to K^-\pi^+$ decays have validated this procedure.

The number of TIS $B_q^0 \to h^+h'^-$ events in each GL bin is obtained from a fit to the inclusive mass distribution [18] assigning the muon mass to the two particles. The measured fractions in each GL bin can be seen in Fig. 1 and are quoted in Table 2. The systematic uncertainties are included, estimated by comparing the results from the inclusive $B_q^0 \to h^+h'^-$ fit model with those obtained using a double Crystal Ball function [19] and a simple background subtraction. The measured GL distribution obtained from TIS $B_q^0 \to h^+h'^-$ events is compatible with a flat distribution, as expected if the simulation reproduces correctly the data.

6.2. Signal invariant mass likelihood

The signal mass lineshape is parameterized using a Crystal Ball function [19]. Two methods have been used to estimate the $B_q^0 \to \mu^+\mu^-$ mass resolution from data. The first of these methods uses an interpolation between the measured resolutions for $c\bar{c}$ resonances (J/ψ, $\psi(2S)$) and $b\bar{b}$ resonances ($\Upsilon(1S)$, $\Upsilon(2S)$, $\Upsilon(3S)$) decaying into two muons. It has been observed that over this mass range the dimuon invariant mass resolution depends linearly on the invariant mass of the muon pair to good approximation. Events selected in the mass ranges around the $c\bar{c}$ and $b\bar{b}$ resonances were weighted such that the momentum spectra of these resonances reproduce the expected momentum spectrum of the b hadron in the decay $B_q^0 \to \mu^+\mu^-$. The mass resolutions of the $c\bar{c}$ and $b\bar{b}$ resonances were then determined fitting a Crystal Ball (J/ψ, $\Upsilon(1S)$) or a Gaussian ($\psi(2S)$, $\Upsilon(2S)$ and $\Upsilon(3S)$) over exponential backgrounds.

The mass resolution is defined as the σ of the Crystal Ball when there is sufficient data to perform a fit with the Crystal Ball function (J/ψ and $\Upsilon(1S)$). Otherwise a Gaussian fit is made ($\psi(2S)$, $\Upsilon(2S)$, $\Upsilon(3S)$) and the σ of the Gaussian is used as an estimator of the σ of the Crystal Ball. For the Crystal Ball function, the parameters describing the radiative tail are in good agreement between data and the Monte Carlo simulation. No systematic shifts in the resolution has been found by using a Crystal Ball or a Gaussian above the transition point.

Interpolating linearly between the five fitted resolutions to $M_{B_s^0}$ an invariant mass resolution of $\sigma = 26.83 \pm 0.14$ MeV/c^2 was estimated for $B_q^0 \to \mu^+\mu^-$. The systematic uncertainty is estimated to be 1 MeV/c^2 mainly due to the reweighting of the momentum spectrum of the dimuon resonances and the variation of the resolution over the width of the $B_q^0 \to \mu^+\mu^-$ signal region.

The second method that was used to estimate the invariant mass resolution from data is to use the inclusive $B_q^0 \to h^+h'^-$ sample. The particle identification requirement would modify the momentum and transverse momentum spectrum of pions and kaons, and thus the mass resolution. Therefore, the fit is performed to the inclusive $B_q^0 \to h^+h'^-$ sample without requiring particle identification and assigning the muon mass to the decay products. The fit has been performed in the GL range [0.25, 1.0] and the results are shown in Fig. 2. The fitted parameters are: the mass resolution, the B^0 and B_s^0 masses, the signal yield, the combinatorial background yields, as well as the fraction of radiative tail and the parameters that describe the combinatorial background. The relative contributions of B^0 and B_s^0 decays are fixed to their known values. The result of the fit for the mass resolution, $\sigma = 25.8 \pm 1.0$ MeV/c^2, is consistent with the value obtained from the interpolation method. However, by varying the assumptions made for the parameters describing the partially reconstructed three-body b-hadron decays (physical background), the estimate obtained for the resolution can change by up to 2.7 MeV/c^2. This is assigned as systematic uncertainty for this method.

The weighted average of the two methods, $\sigma = 26.7 \pm 0.9$ MeV/c^2, is taken as the invariant mass resolution and considered to be the same for B^0 and B_s^0 decays. The mean values of the masses obtained from the inclusive $B_q^0 \to h^+h'^-$ fit are consistent with, but not as precise as, the values obtained using the exclusive decay modes $B^0 \to K^+\pi^-$ and $B_s^0 \to K^+K^-$ isolated using the RICH particle identification: $M_{B^0} = 5275.0 \pm 1.0$ MeV/c^2 and $M_{B_s^0} = 5363.1 \pm 1.5$ MeV/c^2, which are used in the evaluation of the invariant mass likelihood. The mean values of the masses are $\sim 0.07\%$ below the known values [14] which is attributed to a small residual miscalibration of the magnetic field map. However this has no impact on the analysis, provided that the search windows are centred around the measured values.

6.3. Background likelihood

The mass sidebands are defined in the range between $M_{B_q^0} \pm 600$ (1200) MeV/c^2 for the lower (upper) two GL bins, excluding the two search windows ($M_{B_q^0} \pm 60$ MeV/c^2). The background in the mass sidebands is fitted with an exponential function, $f(M) = Ae^{-kM}$. The value of the exponential index k is fitted independently in each GL bin, in order to account for potentially different background compositions. The distribution of the invariant mass for each GL bin is shown in Fig. 3, and the predictions for the numbers of events in the signal regions can be seen in Tables 3 and 4. The background probability in the B_s^0 mass window as a function of GL is shown in Fig. 1 and in Table 2. The results have been checked by fixing the exponential index k to be the same in all GL bins, using a double exponential, or using a simple linear

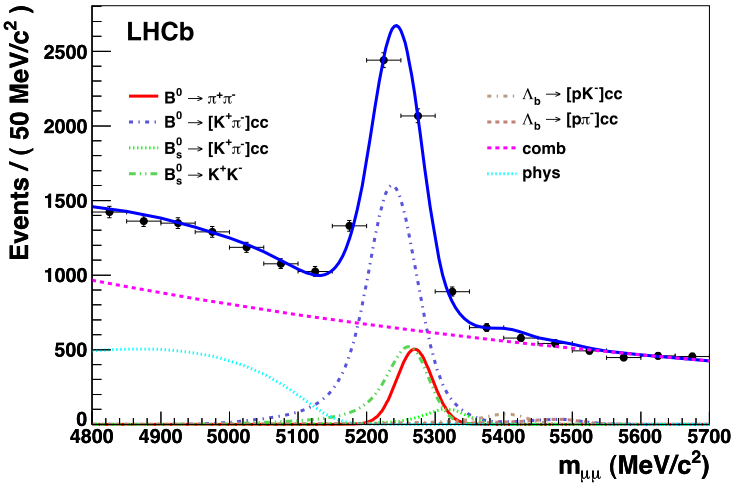

Fig. 2. Fit of the invariant mass distribution for $B_q^0 \to h^+h'^-$ candidates in the GL range [0.25, 1.0]. The pink dashed curve is the combinatorial background component, while the physical background is shown with a light-blue dotted curve. The remaining contributions are from the two-body decays of the B^0, B_s^0 and Λ_b^0. (For interpretation of the references to colour in this figure legend, the reader is referred to the web version of this Letter.)

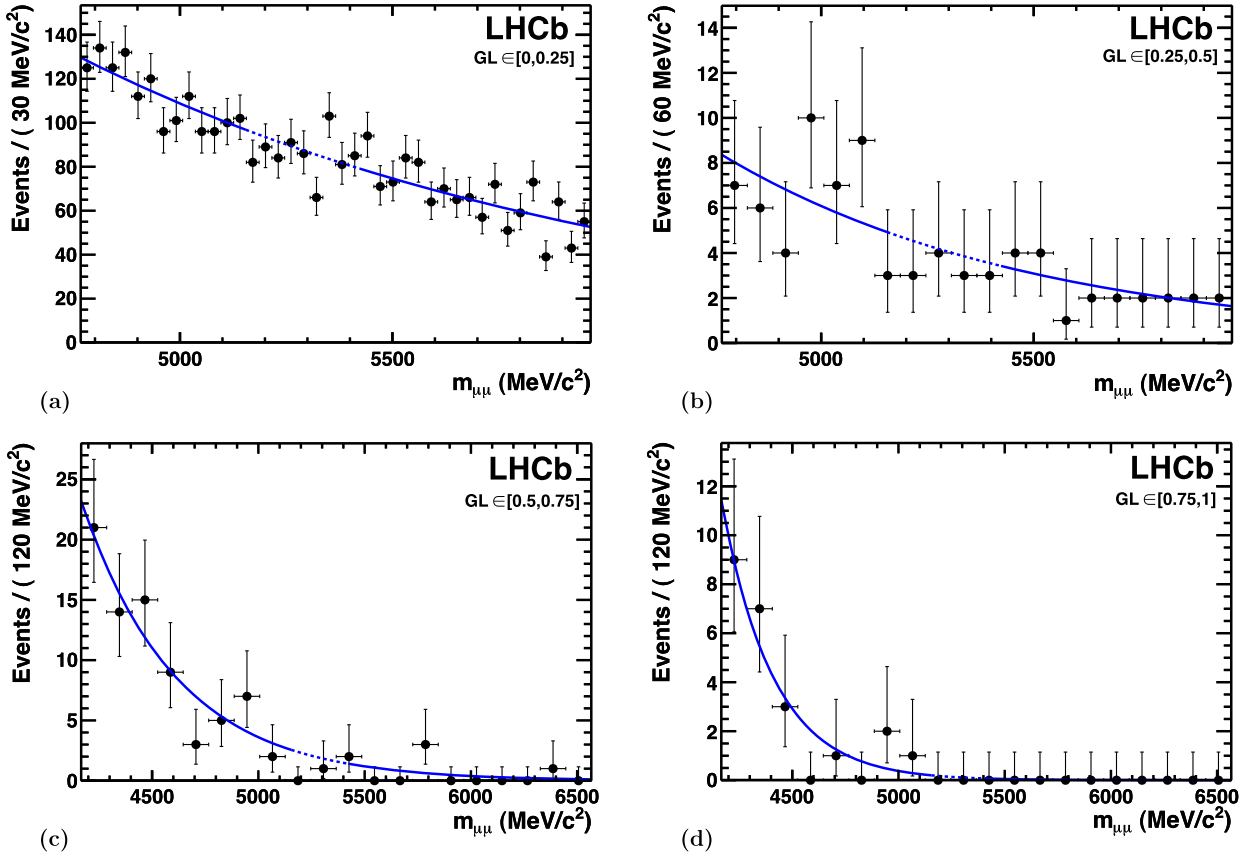

Fig. 3. Distribution of the $\mu\mu$ invariant mass for different GL bins: (a) [0, 0.25], (b) [0.25, 0.5], (c) [0.5, 0.75], (d) [0.75, 1.0]. The blue solid lines show the interpolation model used and the dashed line shows the result of the interpolation in the search windows. (For interpretation of the references to colour in this figure legend, the reader is referred to the web version of this Letter.)

fit in the region around the signal window. In all cases the predicted background is consistent with the result of the exponential fit with different k values, although the quality of the fit is significantly worse when k is forced to be the same for all bins.

7. Results

For each of the 24 bins (4 bins in GL and 6 bins in mass) the expected number of background events is computed from the fits to the invariant mass sidebands described in Section 6.3. The results are shown in Tables 3 and 4. The expected numbers of signal events are computed using the normalization factors from Section 5, and the signal likelihoods computed in Section 6.1 and Section 6.2 for a given value of $\mathcal{B}(B_q^0 \to \mu^+\mu^-)$. The expected numbers of signal events for the SM branching ratios are shown in Tables 3 and 4. The distribution of observed events in the GL *vs* invariant mass plane can be seen in Fig. 4, and the observed number of events in each bin are given in Tables 3 and 4. The

compatibility of the observed distribution of events in the GL *vs* invariant mass plane with a given branching ratio hypothesis is evaluated using the CL_s method [20]. This provides two estimators: CL_s is a measure of the compatibility of the observed distribution with the signal hypothesis, while CL_b is a measure of the compatibility with the background-only hypothesis. The observed distribution of CL_s as a function of the assumed branching ratio can be seen in Fig. 5. The expected distributions of possible values of CL_s assuming the background-only hypothesis are also shown in the same figure as a green shaded area that covers the region of $\pm 1\sigma$ of background compatible observations. The uncertainties in the signal and background likelihoods (Section 6) and normalization factors (Section 5) are used to compute the uncertainties in the background and signal predictions in Tables 3 and 4. These uncertainties are the only source of systematic uncertainty and they are included in the CL_s using the techniques described in Ref. [20]. Given the specific pattern of the observed events, the systematic uncertainty on the background prediction has a negligible effect on the quoted limit. The effect of the uncertainty on the signal prediction increases the quoted limits by less than 3%.

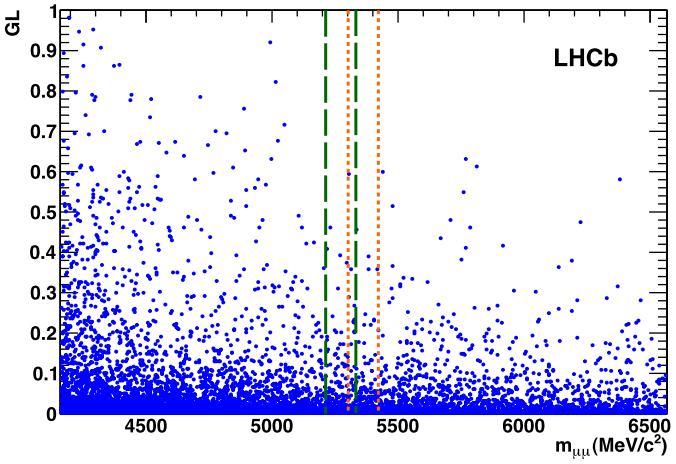

Fig. 4. Observed distribution of selected dimuon events in the GL *vs* invariant mass plane. The orange short-dashed (green long-dashed) lines indicate the ± 60 MeV/c^2 search window around the B_s^0 (B^0). (For interpretation of the references to colour in this figure legend, the reader is referred to the web version of this Letter.)

The evaluation of CL_b [20] gives a probability of about 20% for the compatibility with the background-only hypothesis for both the B_s^0 and B^0 decays. This low value can be attributed to the slight deficit of observed events in the most sensitive bins, as can be seen in Tables 3 and 4. As no significant deviation from the background-only hypothesis is observed, upper limits are computed using the CL_s distributions in Fig. 5 with the results

$$\mathcal{B}\left(B_s^0 \to \mu^+\mu^-\right) < 4.3\ (5.6) \times 10^{-8} \quad \text{at 90\% (95\%) C.L.},$$
$$\mathcal{B}\left(B^0 \to \mu^+\mu^-\right) < 1.2\ (1.5) \times 10^{-8} \quad \text{at 90\% (95\%) C.L.},$$

while the expected values of the limits are $\mathcal{B}(B_s^0 \to \mu^+\mu^-) < 5.1\ (6.5) \times 10^{-8}$ and $\mathcal{B}(B^0 \to \mu^+\mu^-) < 1.4\ (1.8) \times 10^{-8}$ at 90% (95%) C.L. The limits observed are similar to the best published limits [5] for the decay $B_s^0 \to \mu^+\mu^-$ and more restrictive for the decay $B^0 \to \mu^+\mu^-$ [6].

8. Conclusions

With about 37 pb^{-1} of integrated luminosity, LHCb has searched for the rare decays $B_s^0 \to \mu^+\mu^-$ and $B^0 \to \mu^+\mu^-$ and reached sensitivities similar to the existing limits from the Tevatron. This could be achieved due to the large acceptance and trigger efficiency of LHCb, as well as the larger $b\bar{b}$ cross-section in pp collisions at $\sqrt{s} = 7$ TeV. The observed events are compatible with the background expectations, and the upper limits are evaluated to be

$$\mathcal{B}\left(B_s^0 \to \mu^+\mu^-\right) < 5.6 \times 10^{-8} \quad \text{at 95\% C.L.},$$
$$\mathcal{B}\left(B^0 \to \mu^+\mu^-\right) < 1.5 \times 10^{-8} \quad \text{at 95\% C.L.},$$

Table 3
Expected background, expected SM signal and observed number of events in bins of GL and invariant mass, in the ± 60 MeV/c^2 mass window around the B_s^0 mass central value of 5363.1 MeV/c^2.

Invariant mass bin (MeV/c^2)		GL bin [0, 0.25]	[0.25, 0.5]	[0.5, 0.75]	[0.75, 1]
[−60, −40]	Exp. bkg.	$56.9^{+1.1}_{-1.1}$	$1.31^{+0.19}_{-0.17}$	$0.282^{+0.076}_{-0.065}$	$0.016^{+0.021}_{-0.010}$
	Exp. sig.	$0.0076^{+0.0034}_{-0.0030}$	$0.0050^{+0.0027}_{-0.0020}$	$0.0037^{+0.0015}_{-0.0011}$	$0.0047^{+0.0015}_{-0.0010}$
	Observed	39	2	1	0
[−40, −20]	Exp. bkg.	$56.1^{+1.1}_{-1.1}$	$1.28^{+0.18}_{-0.17}$	$0.269^{+0.072}_{-0.062}$	$0.0151^{+0.0195}_{-0.0094}$
	Exp. sig.	$0.0220^{+0.0084}_{-0.0081}$	$0.0146^{+0.0067}_{-0.0054}$	$0.0107^{+0.0036}_{-0.0027}$	$0.0138^{+0.0035}_{-0.0025}$
	Observed	55	2	0	0
[−20, 0]	Exp. bkg.	$55.3^{+1.1}_{-1.1}$	$1.24^{+0.17}_{-0.16}$	$0.257^{+0.069}_{-0.059}$	$0.0139^{+0.0179}_{-0.0086}$
	Exp. sig.	$0.038^{+0.015}_{-0.015}$	$0.025^{+0.012}_{-0.010}$	$0.0183^{+0.0063}_{-0.0047}$	$0.0235^{+0.0060}_{-0.0044}$
	Observed	73	0	0	0
[0, 20]	Exp. bkg.	$54.4^{+1.1}_{-1.1}$	$1.21^{+0.17}_{-0.16}$	$0.246^{+0.066}_{-0.057}$	$0.0128^{+0.0165}_{-0.0080}$
	Exp. sig.	$0.038^{+0.015}_{-0.015}$	$0.025^{+0.012}_{-0.010}$	$0.0183^{+0.0063}_{-0.0047}$	$0.0235^{+0.0060}_{-0.0044}$
	Observed	60	0	0	0
[20, 40]	Exp. bkg.	$53.6^{+1.1}_{-1.0}$	$1.18^{+0.17}_{-0.15}$	$0.235^{+0.063}_{-0.054}$	$0.0118^{+0.0152}_{-0.0073}$
	Exp. sig.	$0.0220^{+0.0084}_{-0.0081}$	$0.0146^{+0.0067}_{-0.0054}$	$0.0107^{+0.0036}_{-0.0027}$	$0.0138^{+0.0035}_{-0.0025}$
	Observed	53	2	0	0
[40, 60]	Exp. bkg.	$52.8^{+1.0}_{-1.0}$	$1.14^{+0.16}_{-0.15}$	$0.224^{+0.060}_{-0.052}$	$0.0108^{+0.0140}_{-0.0068}$
	Exp. sig.	$0.0076^{+0.0031}_{-0.0027}$	$0.0050^{+0.0025}_{-0.0019}$	$0.0037^{+0.0013}_{-0.0010}$	$0.0047^{+0.0013}_{-0.0010}$
	Observed	55	1	0	0

Table 4
Expected background, expected SM signal and observed number of events in bins of GL and invariant mass, in the ± 60 MeV/c^2 mass window around the B^0 central value of 5275.0 MeV/c^2.

Invariant mass bin (MeV/c^2)		GL bin			
		[0, 0.25]	[0.25, 0.5]	[0.5, 0.75]	[0.75, 1]
[−60, −40]	Exp. bkg.	$60.8^{+1.2}_{-1.1}$	$1.48^{+0.19}_{-0.18}$	$0.345^{+0.084}_{-0.073}$	$0.024^{+0.027}_{-0.014}$
	Exp. sig.	$0.00090^{+0.00036}_{-0.00035}$	$0.00060^{+0.00029}_{-0.00023}$	$0.00044^{+0.00016}_{-0.00012}$	$0.00056^{+0.00015}_{-0.00011}$
	Observed	59	2	0	0
[−40, −20]	Exp. bkg.	$59.9^{+1.1}_{-1.1}$	$1.44^{+0.19}_{-0.17}$	$0.329^{+0.080}_{-0.070}$	$0.022^{+0.024}_{-0.013}$
	Exp. sig.	$0.00263^{+0.00093}_{-0.00093}$	$0.00174^{+0.00076}_{-0.00061}$	$0.00128^{+0.00038}_{-0.00030}$	$0.00164^{+0.00035}_{-0.00025}$
	Observed	67	0	0	0
[−20, 0]	Exp. bkg.	$59.0^{+1.1}_{-1.1}$	$1.40^{+0.18}_{-0.17}$	$0.315^{+0.077}_{-0.067}$	$0.020^{+0.022}_{-0.012}$
	Exp. sig.	$0.0045^{+0.0017}_{-0.0017}$	$0.0030^{+0.0014}_{-0.0011}$	$0.00219^{+0.00067}_{-0.00054}$	$0.00280^{+0.00060}_{-0.00045}$
	Observed	56	2	0	0
[0, 20]	Exp. bkg.	$58.1^{+1.1}_{-1.1}$	$1.36^{+0.18}_{-0.16}$	$0.300^{+0.073}_{-0.064}$	$0.019^{+0.021}_{-0.011}$
	Exp. sig.	$0.0045^{+0.0017}_{-0.0017}$	$0.0030^{+0.0014}_{-0.0011}$	$0.00219^{+0.00067}_{-0.00054}$	$0.00280^{+0.00060}_{-0.00045}$
	Observed	60	0	0	0
[20, 40]	Exp. bkg.	$57.3^{+1.1}_{-1.1}$	$1.33^{+0.17}_{-0.16}$	$0.287^{+0.070}_{-0.061}$	$0.017^{+0.019}_{-0.010}$
	Exp. sig.	$0.00263^{+0.00093}_{-0.00093}$	$0.00174^{+0.00076}_{-0.00061}$	$0.00128^{+0.00038}_{-0.00030}$	$0.00164^{+0.00035}_{-0.00025}$
	Observed	42	2	1	0
[40, 60]	Exp. bkg.	$56.4^{+1.1}_{-1.1}$	$1.29^{+0.17}_{-0.16}$	$0.274^{+0.067}_{-0.058}$	$0.0158^{+0.0175}_{-0.0094}$
	Exp. sig.	$0.00090^{+0.00033}_{-0.00032}$	$0.00060^{+0.00027}_{-0.00021}$	$0.00044^{+0.00014}_{-0.00011}$	$0.00056^{+0.00013}_{-0.00010}$
	Observed	49	2	0	0

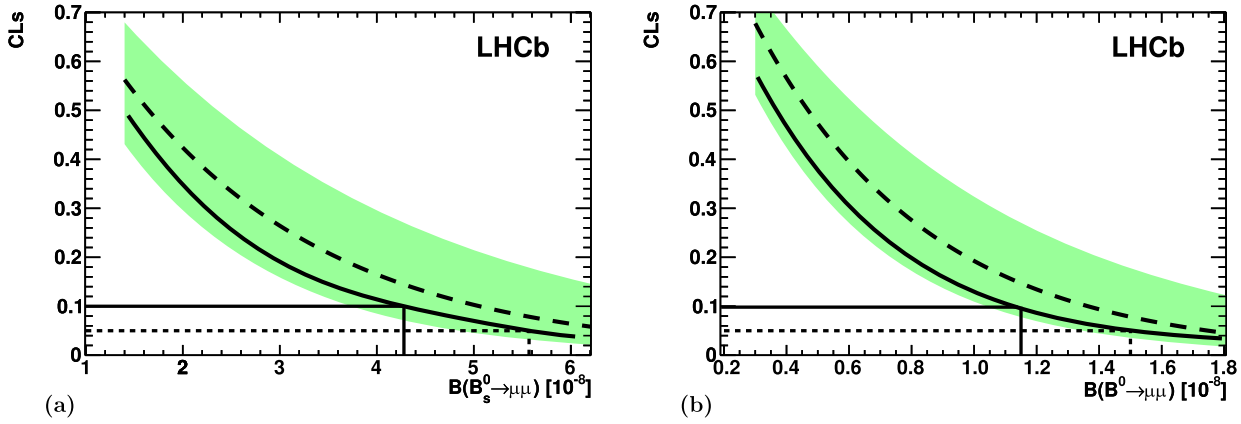

Fig. 5. (a) Observed (solid curve) and expected (dashed curve) CL_s values as a function of $\mathcal{B}(B^0_s \to \mu^+\mu^-)$. The green shaded area contains the $\pm 1\sigma$ interval of possible results compatible with the expected value when only background is observed. The 90% (95%) C.L. observed value is identified by the solid (dashed) line. (b) The same for $\mathcal{B}(B^0 \to \mu^+\mu^-)$. (For interpretation of the references to colour in this figure legend, the reader is referred to the web version of this Letter.)

while the expected values of the limits are $\mathcal{B}(B^0_s \to \mu^+\mu^-) < 6.5 \times 10^{-8}$ and $\mathcal{B}(B^0 \to \mu^+\mu^-) < 1.8 \times 10^{-8}$ at 95% C.L.

The LHC is expected to deliver a much larger sample of pp collisions in 2011. Given the low level of background in the most sensitive bins shown in Tables 3 and 4, LHCb should be able to explore the interesting region of branching ratios at the 10^{-8} level in the near future.

Acknowledgements

We express our gratitude to our colleagues in the CERN accelerator departments for the excellent performance of the LHC. We thank the technical and administrative staff at CERN and at the LHCb institutes, and acknowledge support from the National Agencies: CAPES, CNPq, FAPERJ and FINEP (Brazil); CERN; NSFC (China); CNRS/IN2P3 (France); BMBF, DFG, HGF and MPG (Germany); SFI (Ireland); INFN (Italy); FOM and NWO (Netherlands); SCSR (Poland); ANCS (Romania); MinES of Russia and Rosatom (Russia); MICINN, XUNGAL and GENCAT (Spain); SNSF and SER (Switzerland); NAS Ukraine (Ukraine); STFC (United Kingdom); NSF (USA). We also acknowledge the support received from the ERC under FP7 and the Région Auvergne.

Open access

References

[1] C. Bobeth, et al., Phys. Rev. D 64 (2001) 074014.

[2] G. Buchalla, A.J. Buras, Nucl. Phys. B 548 (1999) 309.
[3] A.J. Buras, Minimal flavour violation and beyond: Towards a flavour code for short distance dynamics, arXiv:1012.1447;
E. Gamiz, et al., Phys. Rev. D 80 (2009) 014503;
A.J. Buras, Phys. Lett. B 566 (2003) 115.
[4] L.J. Hall, R. Rattazzi, U. Sarid, Phys. Rev. D 50 (1994) 7048;
C. Hamzaoui, M. Pospelov, M. Toharia, Phys. Rev. D 59 (1999) 095005;
C.-S. Huang, W. Liao, Q.-S. Yan, Phys. Rev. D 59 (1999) 11701;
S.R. Choudhury, N. Gaur, Phys. Lett. B 451 (1999) 86;
K.S. Babu, C.F. Kolda, Phys. Rev. Lett. 84 (2000) 228.
[5] V. Abazov, et al., D0 Collaboration, Phys. Lett. B 693 (2010) 539.
[6] T. Aaltonen, et al., CDF Collaboration, Phys. Rev. Lett. 100 (2008) 101802.
[7] T. Aaltonen, et al., CDF Collaboration, Search for $B_s^0 \to \mu^+\mu^-$ and $B_d^0 \to \mu^+\mu^-$ decays in 3.7 fb^{-1} of $p\bar{p}$ collisions with CDF II, CDF Public Note 9892.
[8] R. Aaij, et al., LHCb Collaboration, Phys. Lett. B 694 (2010) 209.
[9] A.A. Alves, et al., LHCb Collaboration, JINST 3 (2008) S08005, and references therein.
[10] B. Adeva, et al., LHCb Collaboration, Roadmap for selected key measurements of LHCb, arXiv:0912.4179v2, Chapter 5.
[11] T. Sjöstrand, S. Mrenna, P.Z. Skands, J. High Energy Phys. 0605 (2006) 026.
[12] S. Agostinelli, et al., GEANT4 Collaboration, Nucl. Instrum. Methods A 506 (2003) 250.
[13] D. Martinez Santos, Study of the very rare decay $B_s^0 \to \mu^+\mu^-$ in LHCb, CERN-THESIS-2010-068.
[14] K. Nakamura, et al., Particle Data Group, J. Phys. G 37 (2010) 075021.
[15] D. Asner, et al., Heavy Flavour Averaging Group, Averages of b-hadron, c-hadron, and τ-lepton properties, arXiv:1010.1589. Updated values for f_d/f_s available at http://www.slac.stanford.edu/xorg/hfag/osc/end_2009/ have been used for this Letter, as they include also pre-summer 2010 results which are not contained in [14].
[16] R. Louvot, $\Upsilon(5S)$ results at Belle, arXiv:0905.4345v2.
[17] D. Karlen, Comput. Phys. 12 (1998) 380.
[18] B. Adeva, et al., LHCb Collaboration, Roadmap for selected key measurements of LHCb, arXiv:0912.4179v2, Chapter 3.
[19] J.E. Gaiser, Charmonium spectroscopy from radiative decays of the J/ψ and ψ', PhD thesis, SLAC-R-255, 1982, Appendix F;
T. Skwarnicki, A study of the radiative cascade transitions between the Υ and Υ' resonances, PhD thesis, DESY F31-86-02, 1986, Appendix E.
[20] A.L. Read, J. Phys. G 28 (2002) 2693;
T. Junk, Nucl. Instrum. Methods A 434 (1999) 435.

LHCb Collaboration

R. Aaij [23], B. Adeva [36], M. Adinolfi [42], C. Adrover [6], A. Affolder [48], Z. Ajaltouni [5], J. Albrecht [37], F. Alessio [6,37], M. Alexander [47], P. Alvarez Cartelle [36], A.A. Alves Jr. [22], S. Amato [2], Y. Amhis [38], J. Amoraal [23], J. Anderson [39], R.B. Appleby [50], O. Aquines Gutierrez [10], L. Arrabito [53], M. Artuso [52], E. Aslanides [6], G. Auriemma [22,m], S. Bachmann [11], D.S. Bailey [50], V. Balagura [30,37], W. Baldini [16], R.J. Barlow [50], C. Barschel [37], S. Barsuk [7], A. Bates [47], C. Bauer [10], Th. Bauer [23], A. Bay [38], I. Bediaga [1], K. Belous [34], I. Belyaev [30,37], E. Ben-Haim [8], M. Benayoun [8], G. Bencivenni [18], R. Bernet [39], M.-O. Bettler [17,37], M. van Beuzekom [23], A. Bien [11], S. Bifani [12], A. Bizzeti [17,h], P.M. Bjørnstad [50], T. Blake [49], F. Blanc [38], C. Blanks [49], J. Blouw [11], S. Blusk [52], A. Bobrov [33], V. Bocci [22], A. Bondar [33], N. Bondar [29], W. Bonivento [15], S. Borghi [47], A. Borgia [52], E. Bos [23], T.J.V. Bowcock [48], C. Bozzi [16], T. Brambach [9], J. van den Brand [24], J. Bressieux [38], S. Brisbane [51], M. Britsch [10], T. Britton [52], N.H. Brook [42], H. Brown [48], A. Büchler-Germann [39], A. Bursche [39], J. Buytaert [37], S. Cadeddu [15], J.M. Caicedo Carvajal [37], O. Callot [7], M. Calvi [20,j], M. Calvo Gomez [35,n], A. Camboni [35], P. Campana [18], A. Carbone [14], G. Carboni [21,k], R. Cardinale [19,i], A. Cardini [15], L. Carson [36], K. Carvalho Akiba [23], G. Casse [48], M. Cattaneo [37], M. Charles [51], Ph. Charpentier [37], N. Chiapolini [39], X.Cid Vidal [36], P.J. Clark [46], P.E.L. Clarke [46], M. Clemencic [37], H.V. Cliff [43], J. Closier [37], C. Coca [28], V. Coco [23], J. Cogan [6], P. Collins [37], F. Constantin [28], G. Conti [38], A. Contu [51], M. Coombes [42], G. Corti [37], G.A. Cowan [38], R. Currie [46], B. D'Almagne [7], C. D'Ambrosio [37], W. Da Silva [8], P. David [8], I. De Bonis [4], S. De Capua [21,k], M. De Cian [39], F. De Lorenzi [12], J.M. De Miranda [1], L. De Paula [2], P. De Simone [18], D. Decamp [4], H. Degaudenzi [38,37], M. Deissenroth [11], L. Del Buono [8], C. Deplano [15], O. Deschamps [5], F. Dettori [15,d], J. Dickens [43], H. Dijkstra [37], M. Dima [28], P. Diniz Batista [1], S. Donleavy [48], P. Dornan [49], D. Dossett [44], A. Dovbnya [40], F. Dupertuis [38], R. Dzhelyadin [34], C. Eames [49], S. Easo [45], U. Egede [49], V. Egorychev [30], S. Eidelman [33], D. van Eijk [23], F. Eisele [11], S. Eisenhardt [46], L. Eklund [47], Ch. Elsasser [39], D.G. d'Enterria [35,o], D. Esperante Pereira [36], L. Estève [43], A. Falabella [16,e], E. Fanchini [20,j], C. Färber [11], G. Fardell [46], C. Farinelli [23], S. Farry [12], V. Fave [38], V. Fernandez Albor [36], M. Ferro-Luzzi [37], S. Filippov [32], C. Fitzpatrick [46], F. Fontanelli [19,i], R. Forty [37], M. Frank [37], C. Frei [37], M. Frosini [17,37,f], S. Furcas [20], A. Gallas Torreira [36], D. Galli [14,c], M. Gandelman [2], P. Gandini [51], Y. Gao [3], J.-C. Garnier [37], J. Garofoli [52], L. Garrido [35], C. Gaspar [37], N. Gauvin [38], M. Gersabeck [37], T. Gershon [44], Ph. Ghez [4], V. Gibson [43], V.V. Gligorov [37], C. Göbel [54], D. Golubkov [30], A. Golutvin [49,30,37], A. Gomes [2], H. Gordon [51], C. Gotti [20], M. Grabalosa Gándara [35], R. Graciani Diaz [35], L.A. Granado Cardoso [37], E. Graugés [35], G. Graziani [17], A. Grecu [28], S. Gregson [43], B. Gui [52], E. Gushchin [32], Yu. Guz [34], T. Gys [37], G. Haefeli [38], S.C. Haines [43], T. Hampson [42], S. Hansmann-Menzemer [11], R. Harji [49], N. Harnew [51], P.F. Harrison [44], J. He [7], K. Hennessy [48], P. Henrard [5], J.A. Hernando Morata [36], E. van Herwijnen [37], A. Hicheur [38], E. Hicks [48], W. Hofmann [10], K. Holubyev [11], P. Hopchev [4], W. Hulsbergen [23], P. Hunt [51], T. Huse [48], R.S. Huston [12], D. Hutchcroft [48], V. Iakovenko [7,41], P. Ilten [12], J. Imong [42], R. Jacobsson [37], M. Jahjah Hussein [5], E. Jans [23], F. Jansen [23], P. Jaton [38], B. Jean-Marie [7], F. Jing [3], M. John [51], D. Johnson [51], C.R. Jones [43], B. Jost [37], F. Kapusta [8], T.M. Karbach [9], J. Keaveney [12], U. Kerzel [37], T. Ketel [24], A. Keune [38],

B. Khanji [6], Y.M. Kim [46], M. Knecht [38], S. Koblitz [37], A. Konoplyannikov [30], P. Koppenburg [23], A. Kozlinskiy [23], L. Kravchuk [32], G. Krocker [11], P. Krokovny [11], F. Kruse [9], K. Kruzelecki [37], M. Kucharczyk [25], S. Kukulak [25], R. Kumar [14,37], T. Kvaratskheliya [30,37], V.N. La Thi [38], D. Lacarrere [37], G. Lafferty [50], A. Lai [15], R.W. Lambert [37], G. Lanfranchi [18,*], C. Langenbruch [11], T. Latham [44], R. Le Gac [6], J. van Leerdam [23], J.-P. Lees [4], R. Lefèvre [5], A. Leflat [31,37], J. Lefrançois [7], O. Leroy [6], T. Lesiak [25], L. Li [3], Y.Y. Li [43], L.Li Gioi [5], M. Lieng [9], M. Liles [48], R. Lindner [37], C. Linn [11], B. Liu [3], G. Liu [37], J.H. Lopes [2], E. Lopez Asamar [35], N. Lopez-March [38], J. Luisier [38], B. M'charek [24], F. Machefert [7], I.V. Machikhiliyan [4,30], F. Maciuc [10], O. Maev [29,37], J. Magnin [1], A. Maier [37], S. Malde [51], R.M.D. Mamunur [37], G. Manca [15,37,d], G. Mancinelli [6], N. Mangiafave [43], U. Marconi [14], R. Märki [38], J. Marks [11], G. Martellotti [22], A. Martens [7], L. Martin [51], A. Martín Sánchez [7], D. Martinez Santos [37], A. Massafferri [1], Z. Mathe [12], C. Matteuzzi [20], M. Matveev [29], V. Matveev [34], E. Maurice [6], B. Maynard [52], A. Mazurov [32,37], G. McGregor [50], R. McNulty [12], C. Mclean [46], M. Meissner [11], M. Merk [23], J. Merkel [9], M. Merkin [31], R. Messi [21,k], S. Miglioranzi [37], D.A. Milanes [13,37], M.-N. Minard [4], S. Monteil [5], D. Moran [12], P. Morawski [25], J.V. Morris [45], R. Mountain [52], I. Mous [23], F. Muheim [46], K. Müller [39], R. Muresan [28,38], F. Murtas [18], B. Muryn [26], M. Musy [35], J. Mylroie-Smith [48], P. Naik [42], T. Nakada [38], R. Nandakumar [45], J. Nardulli [45], M. Nedos [9], M. Needham [46], N. Neufeld [37], M. Nicol [7], S. Nies [9], V. Niess [5], N. Nikitin [31], A. Oblakowska-Mucha [26], V. Obraztsov [34], S. Oggero [23], O. Okhrimenko [41], R. Oldeman [15,d], M. Orlandea [28], A. Ostankov [34], B. Pal [52], J. Palacios [39], M. Palutan [18], J. Panman [37], A. Papanestis [45], M. Pappagallo [13,b], C. Parkes [47,37], C.J. Parkinson [49], G. Passaleva [17], G.D. Patel [48], M. Patel [49], S.K. Paterson [49,37], G.N. Patrick [45], C. Patrignani [19,i], C. Pavel-Nicorescu [28], A. Pazos Alvarez [36], A. Pellegrino [23], G. Penso [22,l], M. Pepe Altarelli [37], S. Perazzini [14,c], D.L. Perego [20,j], E. Perez Trigo [36], A. Pérez-Calero Yzquierdo [35], P. Perret [5], A. Petrella [16,37,e], A. Petrolini [19,i], B. Pie Valls [35], B. Pietrzyk [4], D. Pinci [22], R. Plackett [47], S. Playfer [46], M. Plo Casasus [36], G. Polok [25], A. Poluektov [44,33], E. Polycarpo [2], D. Popov [10], B. Popovici [28], C. Potterat [38], A. Powell [51], T. du Pree [23], V. Pugatch [41], A. Puig Navarro [35], W. Qian [3], J.H. Rademacker [42], B. Rakotomiaramanana [38], I. Raniuk [40], G. Raven [24], S. Redford [51], W. Reece [49], A.C. dos Reis [1], S. Ricciardi [45], K. Rinnert [48], D.A. Roa Romero [5], P. Robbe [7], E. Rodrigues [47], F. Rodrigues [2], C. Rodriguez Cobo [36], P. Rodriguez Perez [36], G.J. Rogers [43], V. Romanovsky [34], J. Rouvinet [38], T. Ruf [37], H. Ruiz [35], G. Sabatino [21,k], J.J. Saborido Silva [36], N. Sagidova [29], P. Sail [47], B. Saitta [15,d], C. Salzmann [39], A. Sambade Varela [37], M. Sannino [19,i], R. Santacesaria [22], R. Santinelli [37], E. Santovetti [21,k], M. Sapunov [6], A. Sarti [18], C. Satriano [22,m], A. Satta [21], M. Savrie [16,e], D. Savrina [30], P. Schaack [49], M. Schiller [11], S. Schleich [9], M. Schmelling [10], B. Schmidt [37], O. Schneider [38], A. Schopper [37], M.-H. Schune [7], R. Schwemmer [37], A. Sciubba [18,l], M. Seco [36], A. Semennikov [30], K. Senderowska [26], N. Serra [23], J. Serrano [6], B. Shao [3], M. Shapkin [34], I. Shapoval [40,37], P. Shatalov [30], Y. Shcheglov [29], T. Shears [48], L. Shekhtman [33], O. Shevchenko [40], V. Shevchenko [30], A. Shires [49], E. Simioni [24], H.P. Skottowe [43], T. Skwarnicki [52], A.C. Smith [37], K. Sobczak [5], F.J.P. Soler [47], A. Solomin [42], P. Somogy [37], F. Soomro [49], B. Souza De Paula [2], B. Spaan [9], A. Sparkes [46], E. Spiridenkov [29], P. Spradlin [51], F. Stagni [37], O. Steinkamp [39], O. Stenyakin [34], S. Stoica [28], S. Stone [52], B. Storaci [23], U. Straumann [39], N. Styles [46], M. Szczekowski [27], P. Szczypka [38], T. Szumlak [26], S. T'Jampens [4], V. Talanov [34], E. Teodorescu [28], F. Teubert [37,*], C. Thomas [51,45], E. Thomas [37], J. van Tilburg [39], V. Tisserand [4], M. Tobin [39], S. Topp-Joergensen [51], M.T. Tran [38], A. Tsaregorodtsev [6], N. Tuning [23], A. Ukleja [27], P. Urquijo [52], U. Uwer [11], V. Vagnoni [14], G. Valenti [14], R. Vazquez Gomez [35], P. Vazquez Regueiro [36], S. Vecchi [16], J.J. Velthuis [42], M. Veltri [17,g], K. Vervink [37], B. Viaud [7], I. Videau [7], X. Vilasis-Cardona [35,n], J. Visniakov [36], A. Vollhardt [39], D. Voong [42], A. Vorobyev [29], An. Vorobyev [29], H. Voss [10], K. Wacker [9], S. Wandernoth [11], J. Wang [52], D.R. Ward [43], A.D. Webber [50], M. Whitehead [44], D. Wiedner [11], L. Wiggers [23], G. Wilkinson [51], M.P. Williams [44,45], M. Williams [49], F.F. Wilson [45], J. Wishahi [9], M. Witek [25], W. Witzeling [37], S.A. Wotton [43], K. Wyllie [37], Y. Xie [46], F. Xing [51], Z. Yang [3], G. Ybeles Smit [23], R. Young [46], O. Yushchenko [34], M. Zavertyaev [10,a], L. Zhang [52], W.C. Zhang [12], Y. Zhang [3], A. Zhelezov [11], L. Zhong [3], E. Zverev [31]

[1] *Centro Brasileiro de Pesquisas Físicas (CBPF), Rio de Janeiro, Brazil*
[2] *Universidade Federal do Rio de Janeiro (UFRJ), Rio de Janeiro, Brazil*
[3] *Center for High Energy Physics, Tsinghua University, Beijing, China*
[4] *LAPP, Université de Savoie, CNRS/IN2P3, Annecy-Le-Vieux, France*
[5] *Clermont Université, Université Blaise Pascal, CNRS/IN2P3, LPC, Clermont-Ferrand, France*
[6] *CPPM, Aix-Marseille Université, CNRS/IN2P3, Marseille, France*
[7] *LAL, Université Paris-Sud, CNRS/IN2P3, Orsay, France*

[8] LPNHE, Université Pierre et Marie Curie, Université Paris Diderot, CNRS/IN2P3, Paris, France
[9] Fakultät Physik, Technische Universität Dortmund, Dortmund, Germany
[10] Max-Planck-Institut für Kernphysik (MPIK), Heidelberg, Germany
[11] Physikalisches Institut, Ruprecht-Karls-Universität Heidelberg, Heidelberg, Germany
[12] School of Physics, University College Dublin, Dublin, Ireland
[13] Sezione INFN di Bari, Bari, Italy
[14] Sezione INFN di Bologna, Bologna, Italy
[15] Sezione INFN di Cagliari, Cagliari, Italy
[16] Sezione INFN di Ferrara, Ferrara, Italy
[17] Sezione INFN di Firenze, Firenze, Italy
[18] Laboratori Nazionali dell'INFN di Frascati, Frascati, Italy
[19] Sezione INFN di Genova, Genova, Italy
[20] Sezione INFN di Milano Bicocca, Milano, Italy
[21] Sezione INFN di Roma Tor Vergata, Roma, Italy
[22] Sezione INFN di Roma La Sapienza, Roma, Italy
[23] Nikhef National Institute for Subatomic Physics, Amsterdam, Netherlands
[24] Nikhef National Institute for Subatomic Physics and Vrije Universiteit, Amsterdam, Netherlands
[25] Henryk Niewodniczanski Institute of Nuclear Physics Polish Academy of Sciences, Cracow, Poland
[26] Faculty of Physics & Applied Computer Science, Cracow, Poland
[27] Soltan Institute for Nuclear Studies, Warsaw, Poland
[28] Horia Hulubei National Institute of Physics and Nuclear Engineering, Bucharest-Magurele, Romania
[29] Petersburg Nuclear Physics Institute (PNPI), Gatchina, Russia
[30] Institute of Theoretical and Experimental Physics (ITEP), Moscow, Russia
[31] Institute of Nuclear Physics, Moscow State University (SINP MSU), Moscow, Russia
[32] Institute for Nuclear Research of the Russian Academy of Sciences (INR RAN), Moscow, Russia
[33] Budker Institute of Nuclear Physics (BINP), Novosibirsk, Russia
[34] Institute for High Energy Physics (IHEP), Protvino, Russia
[35] Universitat de Barcelona, Barcelona, Spain
[36] Universidad de Santiago de Compostela, Santiago de Compostela, Spain
[37] European Organization for Nuclear Research (CERN), Geneva, Switzerland
[38] Ecole Polytechnique Fédérale de Lausanne (EPFL), Lausanne, Switzerland
[39] Physik-Institut, Universität Zürich, Zürich, Switzerland
[40] NSC Kharkiv Institute of Physics and Technology (NSC KIPT), Kharkiv, Ukraine
[41] Institute for Nuclear Research of the National Academy of Sciences (KINR), Kyiv, Ukraine
[42] H.H. Wills Physics Laboratory, University of Bristol, Bristol, United Kingdom
[43] Cavendish Laboratory, University of Cambridge, Cambridge, United Kingdom
[44] Department of Physics, University of Warwick, Coventry, United Kingdom
[45] STFC Rutherford Appleton Laboratory, Didcot, United Kingdom
[46] School of Physics and Astronomy, University of Edinburgh, Edinburgh, United Kingdom
[47] School of Physics and Astronomy, University of Glasgow, Glasgow, United Kingdom
[48] Oliver Lodge Laboratory, University of Liverpool, Liverpool, United Kingdom
[49] Imperial College London, London, United Kingdom
[50] School of Physics and Astronomy, University of Manchester, Manchester, United Kingdom
[51] Department of Physics, University of Oxford, Oxford, United Kingdom
[52] Syracuse University, Syracuse, NY, United States
[53] CC-IN2P3, CNRS/IN2P3, Lyon-Villeurbanne, France [p]
[54] Pontifícia Universidade Católica do Rio de Janeiro (PUC-Rio), Rio de Janeiro, Brazil [q]

* Corresponding authors.
E-mail addresses: gaia.lanfranchi@lnf.infn.it (G. Lanfranchi), Frederic.Teubert@cern.ch (F. Teubert).
[a] P.N. Lebedev Physical Institute, Russian Academy of Science (LPI RAS), Moscow, Russia.
[b] Università di Bari, Bari, Italy.
[c] Università di Bologna, Bologna, Italy.
[d] Università di Cagliari, Cagliari, Italy.
[e] Università di Ferrara, Ferrara, Italy.
[f] Università di Firenze, Firenze, Italy.
[g] Università di Urbino, Urbino, Italy.
[h] Università di Modena e Reggio Emilia, Modena, Italy.
[i] Università di Genova, Genova, Italy.
[j] Università di Milano Bicocca, Milano, Italy.
[k] Università di Roma Tor Vergata, Roma, Italy.
[l] Università di Roma La Sapienza, Roma, Italy.
[m] Università della Basilicata, Potenza, Italy.
[n] LIFAELS, La Salle, Universitat Ramon Llull, Barcelona, Spain.
[o] Institució Catalana de Recerca i Estudis Avançats (ICREA), Barcelona, Spain.
[p] Associated member.
[q] Associated to Universidade Federal do Rio de Janeiro (UFRJ), Rio de Janeiro, Brazil.